Journal of Magnetic Resonance 213 (2011) 200–205

Contents lists available at SciVerse ScienceDirect

Journal of Magnetic Resonance

journal homepage: www.elsevier.com/locate/jmr

Communication

Nonselective excitation of pulsed ELDOR using multi-frequency microwaves

Yuki Asada [a], Risa Mutoh [b,c], Masahiro Ishiura [b,c], Hiroyuki Mino [a,*]

[a] Division of Material Science (Physics), Graduate School of Science, Nagoya University, Furo, Chikusa, Nagoya 464-8602, Japan
[b] Division of Biological Science, Graduate School of Science, Nagoya University, Furo, Chikusa, Nagoya 464-8602, Japan
[c] Center for Gene Research, Nagoya University, Furo, Chikusa, Nagoya 464-8602, Japan

ARTICLE INFO

Article history:
Received 29 May 2011
Revised 9 September 2011
Available online 17 September 2011

Keywords:
Pulsed EPR
ELDOR
PELDOR
DEER
Site-directed spin labeling

ABSTRACT

The use of a polychromatic microwave pulse to expand the pumping bandwidth in pulsed electron–electron double resonance (PELDOR) was investigated. The pumping pulse was applied in resonance with the broad (~100 mT) electron paramagnetic resonance (EPR) signal of the manganese cluster of photosystem II in the S_2 state. The observation pulses were in resonance with the narrow EPR signal of the tyrosine radical, $Y_D^{\bullet}$. It was found that in the case of the polychromatic pumping pulse containing five harmonics with the microwave frequencies between 8.5 and 10.5 GHz the PELDOR effect corresponding to the dipole interaction between the Mn cluster and $Y_D^{\bullet}$ was about 2.9 times larger than that achieved with a monochromatic pulse. In addition to the dipolar modulation, the nuclear modulation effects were observed. The effects could be suppressed by averaging the PELDOR trace over the time interval between the observation microwave pulses. The polychromatic excitation technique described will be useful for improving the PELDOR sensitivity in the measurements of long distances in biological samples, where the pair consists of a radical with a narrow EPR spectrum and slow phase relaxation, and a metal center that has a broad EPR spectrum and a short phase relaxation time.

© 2011 Elsevier Inc. All rights reserved.

1. Introduction

Pulsed electron–electron double resonance (PELDOR, also called double electron–electron resonance, DEER) is a powerful pulsed electron paramagnetic resonance (EPR) technique for elucidating macromolecular structure through measurements of magnetic dipole interactions between paramagnetic centers, reviewed in [1]. It has recently become a routine method in protein research because of advancement of the site-directed spin labeling (SDSL) technique [2]. Specifically for the SDSL applications, the optimal PELDOR techniques are well established, as well as the alternative pulsed EPR approach based on exciting a double quantum coherence (DQC) [3] between the two nitroxide spin labels.

In many biological applications, the situation is encountered when a protein contains two paramagnetic metal centers or a metal center and an organic radical. In such cases, the specifics of the optimal PELDOR application may depend on the system (see, e.g. [4]). The increased EPR linewidth generally results in lower sensitivity of PELDOR measurements, especially since the concentration of the biological samples is usually limited. In addition, if the Zeeman or hyperfine interaction (*hfi*) anisotropy determines the EPR linewidth, the effects of orientational selectivity may complicate the PELDOR measurements.

Recently, an elegant PELDOR technique utilizing magnetic field jumps and high repetition rate data acquisition was suggested for overcoming these difficulties in the case of both centers having broad EPR spectra [5].

In this work, we concentrate on a situation of a pair consisting of the centers with a broad and narrow EPR spectrum. In such a situation, if the center with a narrow spectrum (a radical) has a significantly longer phase relaxation time that its wide-spectrum counterpart (a transition metal center), it may be advantageous in PELDOR measurements to observe the electron spin echo (ESE) signal of the radical, while pumping the broad EPR signal. Since the pumping pulse bandwidth is limited and is usually much smaller than the metal center EPR linewidth, the efficiency of this "inverted" implementation of PELDOR can be rather low. Therefore, we investigated a possibility to improve the sensitivity of this kind of PELDOR measurements by using multifrequency (polychromatic) pumping pulses, which can significantly expand the pumping bandwidth. As a model system, we used the plant photosystem II (PS II) in the S_2 state [6]. The tyrosine radical, $Y_D^{\bullet}$, and the Mn cluster are located in the same PS II protein complex as a pair.

Abbreviations: EPR, electron paramagnetic resonance; PELDOR, pulsed electron–electron double resonance; DEER, double electron–electron resonance; ESE, electron spin echo; CW, continuous wave; MW, microwave; S/N, signal-to-noise; TWTA, traveling-wave tube amplifier; PS II, photosynthetic protein photosystem II.

* Corresponding author. Fax: +81 52 789 2882.
E-mail address: mino@bio.phys.nagoya-u.ac.jp (H. Mino).

1090-7807/$ - see front matter © 2011 Elsevier Inc. All rights reserved.
doi:10.1016/j.jmr.2011.09.034

The internal structure is fixed, so fine PELDOR oscillation patterns can be observed clearly, without consideration of distribution over distances [6].

2. Experimental

2.1. Sample preparation

PS II membranes were prepared from spinach according to the method previously described, [7] with a slight modification [8]. The membranes were dissolved in a medium containing 400 mM sucrose, 15 mM NaCl, 5 mM MgCl and 40 mM Mes/NaOH (pH 6.5). The membranes were transferred into quartz EPR tubes, illuminated for 5 min with white light (POT-150, ASAHI SPECTRA) at 200 K, and rapidly cooled to 77 K [6].

2.2. EPR measurements

ESE experiments were performed on a pulsed EPR spectrometer ESP-380E (Bruker). The spectrometer was equipped with a cylindrical dielectric cavity (ER4117DHQ-H, Bruker) and a gas flow temperature control system (CF935, Oxford Instruments). The 1 kW TWTA with the bandwidth of 8.0–12.4 GHz was used (model117, Applied System Engineering). Mw pulses of 16 and 24 ns durations were used for the $\pi/2$ and π flip angles, respectively. The field-sweep ESE spectra were measured by the $\pi/2$–τ–π sequence with a time interval τ of 200 ns between the mw pulses. For PELDOR measurements, the $\pi/2$–τ–π sequence with a time interval τ of 1000 or 1200 ns between the mw pulses from the ESP380 source was used for observation, while a mw pulse of 24 or 56 ns from the second mw source was used for pumping. The second (pumping) mw source was either a mw synthesizer (HP83751A, Hewlett–Packard) or the home-made mw source described below. The specifications of the home-made mw source were evaluated using the spectral analyzer (MS2687B, Anritsu).

2.3. The multifrequency mw source

Fig. 1 shows the block diagram of the home-made mw source supplying the multi-frequency (polychromatic) microwaves. Five local microwave (mw) generators (HMC-C030, Hittite), denoted as oscillator n (n = 1–5), were used. The mw frequency for each local oscillator is adjustable within the range of 8–11 GHz. The outputs of the local generators are combined using a mw combiner (A8338-8, GHZ TECHNOLOGIES), preamplified using a driver amplifier (APT10555M51, Avantek), and fed to the pulse former unit corresponding to channel ⟨X⟩ in the mw bridge of ESP380E.

Fig. 2 shows an example of the power spectrum at the output of the driver amplifier. The five large (~12 dbm) peaks correspond to the main harmonics of the local mw oscillators. The numerous peaks from minor harmonics have negligible amplitude of about −20 dbm.

3. Results and discussion

In PELDOR, a two-pulse (primary) or three-pulse (refocused primary) electron spin echo (ESE) sequence is applied to detect the ESE signal from one of the spins (spin A) in a dipole-coupled pair of paramagnetic centers. The other center in the pair, spin B, is flipped (turned by 180°) by a pumping mw pulse of a different carrier frequency, which changes the local magnetic field for spin A and alters its ESE amplitude (ELDOR effect). The dipole interaction is evaluated from the dependence of spin A ESE amplitude on the position of the pumping pulse with respect to the observation pulses. For the pair with a fixed distance between spins A and B, R_{AB}, this dependence is oscillatory, with the characteristic frequency equal to the dipole interaction constant.

In this work, the three-pulse PELDOR sequence shown in Fig. 3 was used. Fig. 3A shows the observation mw pulses with the frequency ν_1 used for the detection of the ESE signal of spin A. Fig. 3B shows the pumping mw pulse with the frequency ν_2 used for the inversion of spin B.

The ESE amplitude depends on the interval τ' between the first and second pulses [6,9–11] (see Fig. 3) as:

$$V(\tau') = 1 - C[1 - \cos(2\pi D\tau')] \quad (1)$$

where C is the fraction of spins B flipped by the pumping pulse, and D is the dipole interaction between the two spins:

$$D = D_o(1 - 3\cos^2\theta_R) \quad (2)$$

In the last expression, θ_R is the angle between the external magnetic field, $\mathbf{B_o}$, and the radius-vector, $\mathbf{R}$, joining spins A and B. The dipole interaction constant, D_o, is given by:

$$D_o = g_A g_B \beta^2 / hR^3 \quad (3)$$

where g_A and g_B are the g-factors of spins A and B, β is the Bohr magneton, and h is the Planck constant. In an orientationally disordered system, Eq. (1) has to be averaged over θ_R.

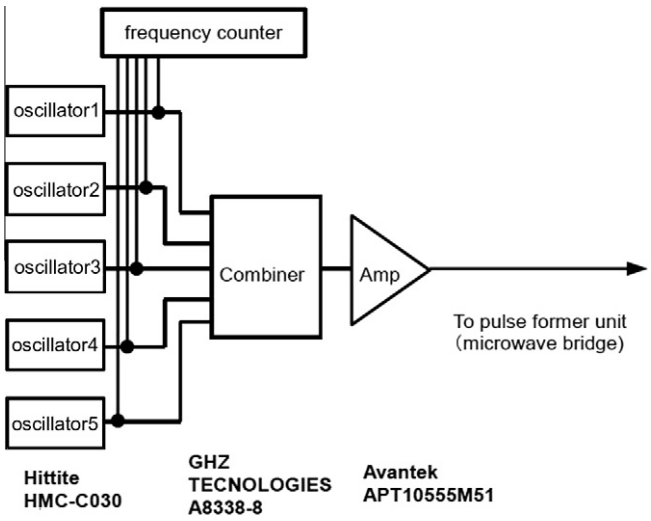

Fig. 1. Simplified block diagram of the multi-frequency mw source.

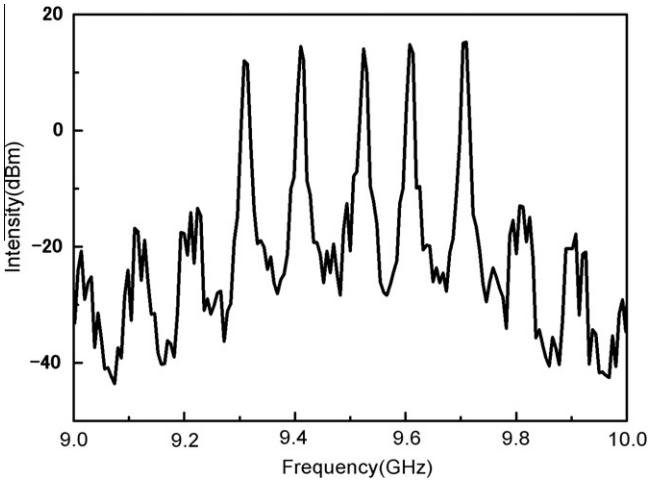

Fig. 2. Power spectrum of the output of the multi-frequency mw source shown in Fig. 1. The five large peaks represent the main harmonics of the five mw oscillators; their frequencies are adjustable within the range of 8.5–10.5 GHz.

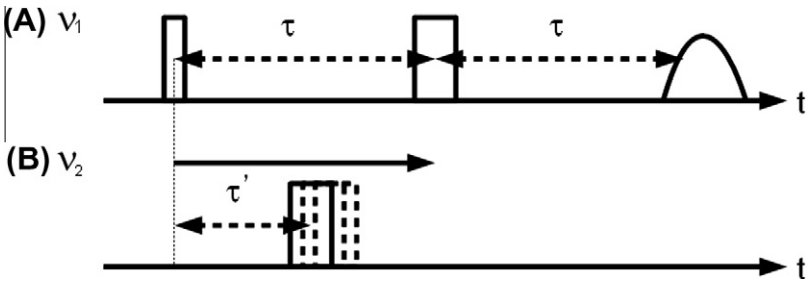

Fig. 3. Pulse sequence for the three-pulse PELDOR. (A) A spin echo signal from spin A is generated by observation sequence consisting of two mw pulses with the carrier mw frequency ν_1, separated by the time interval τ. (B) The spin B is inverted by the pumping mw pulse with the carrier mw frequency ν_2. In the experiment, the observation time interval τ is kept constant, and the ESE signal amplitude is measured as a function of the pumping pulse position, τ', which is the time interval between the first observation pulse and the pumping pulse.

If the paramagnetic centers in the pair have significantly different EPR linewidths, the center with a more broad EPR spectrum is traditionally used for observation (as spin A), while the center with a more narrow spectrum is used for pumping (spin B). In addition, the pumping frequency, ν_2, is usually set to correspond to the optimal frequency of the resonator. This relative arrangement of the pumping and observation frequencies seeks to maximize the spin flip probability for the pumping pulse (the factor C in Eq. (1)), and thus to maximize the achievable amplitude of the ELDOR effect.

In some cases, however, the narrow spectrum corresponds to an organic radical characterized by a relatively long phase relaxation time, T_{2R}, and the broad spectrum corresponds to a transition metal ion that might have a much shorter T_{2M}. If T_{2M} is shorter than the characteristic period of the dipolar oscillations observed by PELDOR ($T_{2M} < 1/D_o$), then the traditional frequency arrangement in the PELDOR experiment may not result in successful measurement of the distance. If in this case $T_{2R} > 1/D_o$, it may be advantageous to designate the radical as spin A and the metal center as spin B. An example of such an "inverted" implementation of PELDOR is considered below.

Fig. 4A shows the ESE field-sweep spectrum of PS II in the S_2 state. The sharp signal around $g = 2$ with 2 mT width arises from a tyrosine radical known as $Y_D^{\bullet}$. The broad signal with >60 mT width is the so-called multiline signal arising from the Mn cluster in the S_2-state. In this state, the Mn cluster has spin $S = 1/2$, and its g-factor is nearly isotropic. Fig. 4B shows the PELDOR trace obtained using a traditional implementation of PELDOR, with ν_2 being in resonance with the narrow signal of $Y_D^{\bullet}$ and ν_1 in resonance with the broad signal of the Mn cluster. The oscillations with the characteristic frequency of about 2.5 MHz observed in this trace are caused by the dipole interaction between the Mn cluster and $Y_D^{\bullet}$ [6]. The dotted line in Fig. 4B is the ELDOR trace simulated for the distance $R = 27$ Å.

Let us consider now the inverted implementation of PELDOR, with ν_1 being at the resonator optimum and in resonance with $Y_D^{\bullet}$ (spin A), and ν_2 being away from the resonator optimum and in resonance with the Mn cluster (spin B). In principle, this frequency arrangement seeks to extend the PELDOR detection interval τ as much as possible, and thus to maximize the detectable distances between spins A and B (although at the expense of the lower ELDOR effect and increase of the data accumulation time). In this work, however, we did not pursue this goal and were mostly concerned with the amplitude of the ELDOR effect.

In the inverted implementation, the efficiency of the pumping pulse depends on its mw frequency because of the non-zero quality factor (Q-value) of the resonator. Fig. 5 shows (A) the dependence of the ELDOR effect on ν_2 and (B) the ESE field-sweep spectrum of PS II in the S_2 state, which is the expansion of the spectrum shown in Fig. 4A. The horizontal axis in panel B is scaled to provide a correspondence between the magnetic fields and the mw frequencies in panel A. In this experiment, the observation pulses were in resonance with $Y_D^{\bullet}$, and the pumping pulse was in resonance with the Mn multiline signal. As a measure of the ELDOR

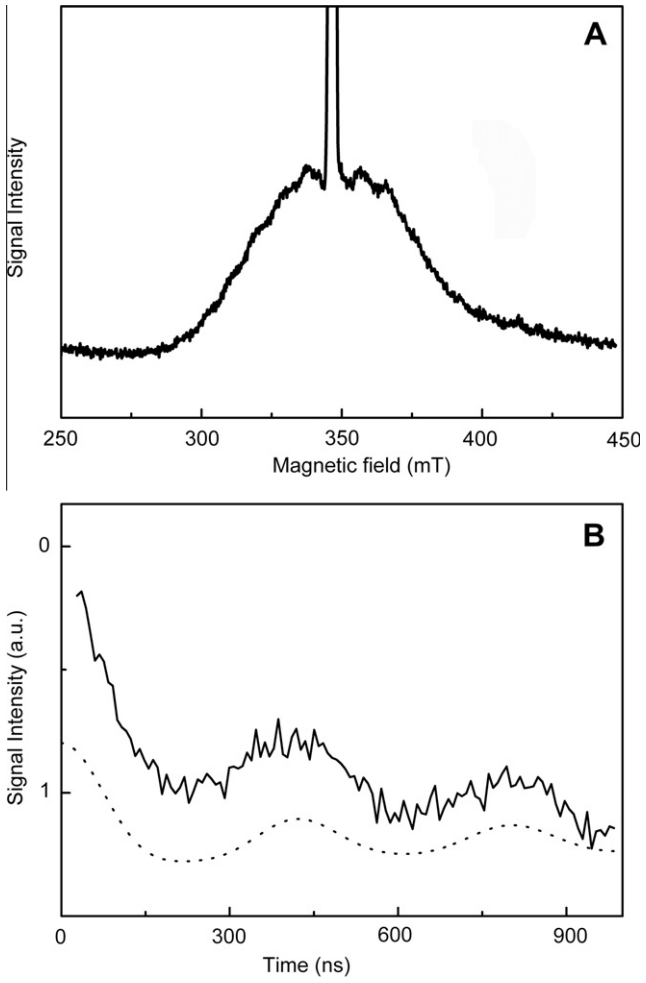

Fig. 4. (A) Two-pulse ESE field-sweep spectrum of PS II membranes. Experimental conditions: mw frequency, 9.59 GHz; pulse lengths, 16 ns for $\pi/2$ pulses and 24 ns for π pulses; time interval between the mw pulses, $\tau = 200$ ns; pulse repetition time, 2 ms; temperature, 4 K. (B) PELDOR spectrum arising from the interaction between $Y_D^{\bullet}$ and the Mn cluster. The initial intensity was set to the starting point (zero). Experimental conditions: observation mw frequency, $\nu_1 = 9.79$ GHz; pumping mw frequency, $\nu_2 = 9.62$ GHz (supplied from HP83751A); observation time interval, $\tau = 1000$ ns; $B_o = 343.8$ mT; temperature, 4 K. Dashed line shows the simulation of the PELDOR trace assuming the distance $R = 27$ Å between localized spin $S = 1/2$ centers.

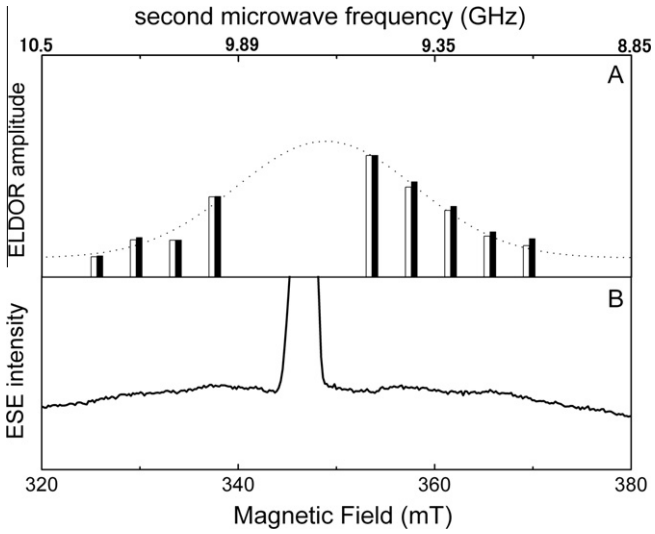

Fig. 5. (A) Filled bars show the dependence of the PELDOR effect on the mw frequency of the pumping pulse (ν_2, in resonance with the Mn multiline signal). The observation frequency, ν_1, was in resonance with $Y_D^{\bullet}$. Open bars show the PELDOR effects normalized by ESE amplitudes of the Mn multiline signal shown in panel B. Dotted line represents a Gaussian fit to the frequency dependence shown by the open bars. The Gaussian line is centered at 9.65 GHz and has a width of 500 MHz (~18 mT). Experimental conditions: ν_1 = 9.70 GHz; B_o = 347.0 mT. The other conditions are the same as in Fig. 4B. (B) rescaled ESE field-sweep spectrum from Fig. 4A, where the magnetic field was calculated to correspond to ν_2 in panel A.

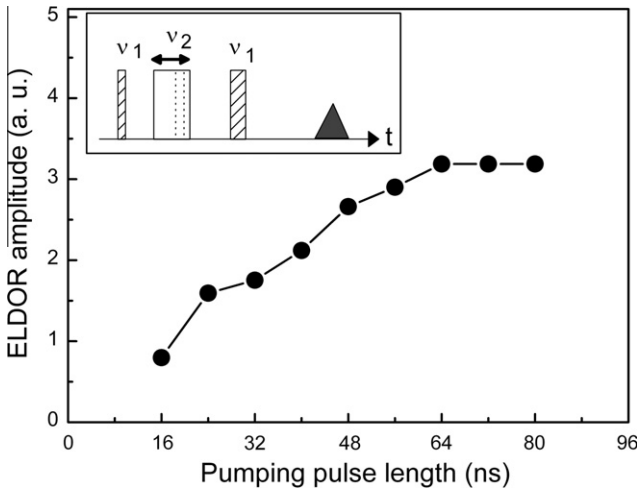

Fig. 6. The pumping pulse length dependence of PELDOR amplitude caused by the dipole interaction between $Y_D^{\bullet}$ and Mn cluster. The first and third pulses were in resonance with $Y_D^{\bullet}$, while the pumping pulse was in resonance with the Mn multiline signal. The five combined microwaves were used for the pumping pulse, and the pulse length was changed in the range of 16–80 ns. The PELDOR amplitudes were evaluated by the amplitude of the first oscillation period. *Inset* shows the pulse sequence. Experimental conditions: ν_1 = 9.60 GHz; ν_2 = 9.36, 9.38, 9.40, 9.42 and 9.44 GHz, supplied from the multifrequency mw source; B_o = 343.0 mT; temperature, 4 K; pulse lengths for ν_1, 16 ns and 24 ns; interval τ, 1000 ns.

effect in panel A of Fig. 5, the oscillation amplitude in the first oscillation period in the PELDOR trace ($\tau' < 500$ ns) was used. Filled bars show the PELDOR amplitudes as obtained in the experiment, while the open bars are obtained by normalizing the experimental PELDOR amplitudes by the corresponding ESE intensities of the Mn multiline signal.

The frequency dependence of the normalized PELDOR amplitudes (open bars) was fitted by a Gaussian function (dotted line). This function is centered at 9.65 GHz and has with a width of 500 MHz (~18 mT) between the maximum slope points. The frequency dependence shown in Fig. 5 gives an idea about the relative sensitivities of PELDOR experiments performed with different offsets of ν_2 from the resonator optimum.

Fig. 6 shows the $Y_D^{\bullet}$ ELDOR amplitude as a function of the pumping pulse length obtained for one specific set of the five pumping frequencies (see figure caption for details). The maximum ELDOR amplitude (measured as the amplitude of the first oscillation in the PELDOR trace) was obtained for the pumping pulse length of 56 ns, and it decreased for the pulse length of more than 64 ns. Therefore, we estimated the length of the pumping π pulse as 56 ns.

Fig. 7 shows the PELDOR traces obtained with the observation pulses in resonance with $Y_D^{\bullet}$ and the pumping pulse in resonance with the Mn multiline signal. Traces *a*–*c* were measured under the same experimental conditions, except for the frequency composition of the pumping pulse: (*a*) one, (*b*) two, and (*c*) five mw frequencies. While the oscillations seen in these PELDOR traces are rather similar to the oscillation in the "normal" PELDOR trace of Fig. 4B, some distortions are obvious. In order to understand the nature of these distortions, the Fourier transformation (FT) spectra of these PELDOR traces were calculated (Fig. 8). As seen in Fig. 8, all of the spectra contain a major peak at 2.5 MHz caused by the dipole interaction between $Y_D^{\bullet}$ and the Mn cluster. In addition, the spectra obtained using the inverted implementation of PELDOR show the lines at ~15 and ~5 MHz. The 15 MHz line represents the electron spin echo envelope modulation (ESEEM) caused by the interaction of the unpaired electrons of $Y_D^{\bullet}$ and the Mn cluster with protons, while the 5 MHz line is caused by the interaction of the Mn cluster with the nearby ^{14}N nucleus (similar frequency is observed in the usual ESEEM spectra of the Mn cluster [12]).

The observation of the nuclear ESEEM is a common feature of PELDOR experiments under certain conditions (insufficient frequency separation between the observation and pumping pulses, approximate matching of the electron spin nutation frequency under the pumping mw field with the nuclear hyperfine interaction) [13], and the common technique to suppress this ESEEM consists in detecting the PELDOR traces at different time intervals of the observation sequence (in the case of three pulse PELDOR, τ), and adding all of the traces together. As an example, trace *d* (dotted line) in Fig. 7 represents such a τ-averaged PELDOR trace obtained with the five-frequency pumping pulse (same as trace *c* in the same figure). The FT spectrum of the τ-averaged PELDOR trace is shown by trace *d* in Fig. 8. One can see that the ^1H ESEEM peak in this trace is suppressed. The ^{14}N line is not suppressed because the averaging timebase was too small (the variation in τ was only 72 ns). The reason why this line is observed is that the observation pulses are not only in resonance with $Y_D^{\bullet}$, but also with the central part of the Mn cluster spectrum.

Experiments with other separations between the observation and pumping frequencies have shown that the nuclear ESEEM (especially the ^1H ESEEM) has increased dramatically for smaller frequency separations between the observation and pumping pulses (data not shown). We can conclude therefore, that because of small amplitude and relatively large length of the pumping pulses in the inverted implementation of PELDOR, the nuclear ESEEM becomes a nearly unavoidable feature, and the experiments with averaging over the observation sequence time interval(s) are necessary to suppress this ESEEM.

A comparison of the normalized (by the initial ESE amplitude) PELDOR amplitudes in Fig. 7 shows that their ratio for traces *a*:*b*:*c* is approximately 1:1.4:2.9. In order to qualitatively understand this ratio, one has to know the response of TWTA to a pulsed multifrequency excitation. Two limiting cases can be considered. In the first case, the TWTA is saturated, producing the fixed overall output power *P*. In the case of a multifrequency pulse consisting of *N* harmonics, the power allocation for one harmonic is then *P*/

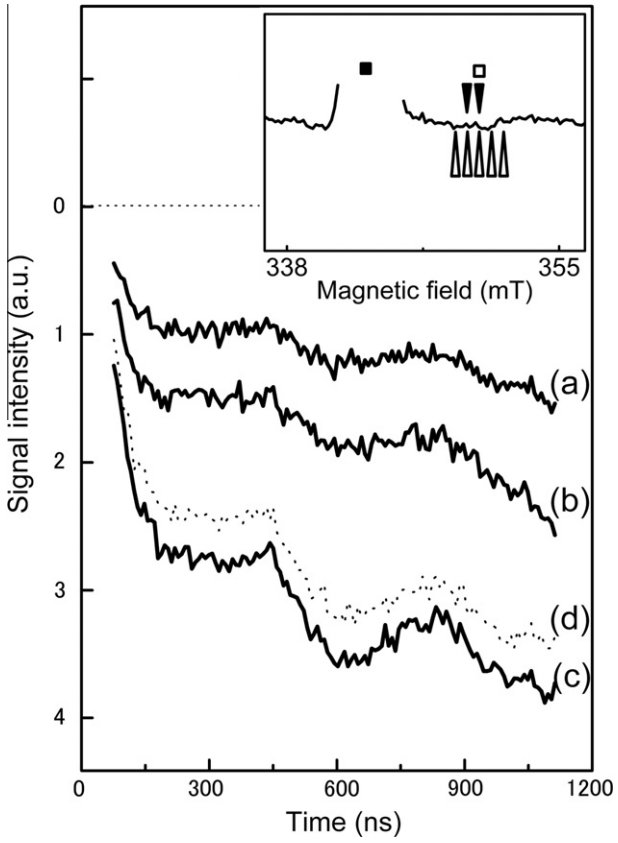

Fig. 7. PELDOR traces obtained with ν_1 in resonance with $Y_D^{\bullet}$ and ν_2 in resonance with the Mn multiline signal. Traces *a*–*c* were measured under the same experimental conditions except for the pumping pulse with (*a*) a single, (*b*) two and (*c*) five mw sources. The initial intensity was set to the starting point (zero). Trace *d* is a sum of the traces at five different τ (=1200, 1216, 1232, 1248 and 1274 ns) obtained with five mw sources, where the ELDOR amplitudes were normalized by ESE amplitudes. These microwaves were supplied from the multifrequency mw source. *Inset:* the expansion of Fig. 4A showing the observation and pumping positions. Filled square shows the observation frequency, ν_1. Open square, filled and blank triangles show the pumping mw frequencies (ν_2) for one, two, and five mw sources, respectively. Experimental conditions: ν_1 = 9.60 GHz; ν_2 = 9.40 GHz (trace *a*), 9.40 and 9.42 GHz (trace *b*), and 9.36, 9.38, 9.40, 9.42, and 9.44 GHz (trace *c*); B_o = 343.0 mT; temperature, 4 K; pulse lengths for ν_1, 16 and 24 ns; pulse length for ν_2, 56 ns; τ = 1200 ns for traces *a*–*c*; accumulations, 1000 times.

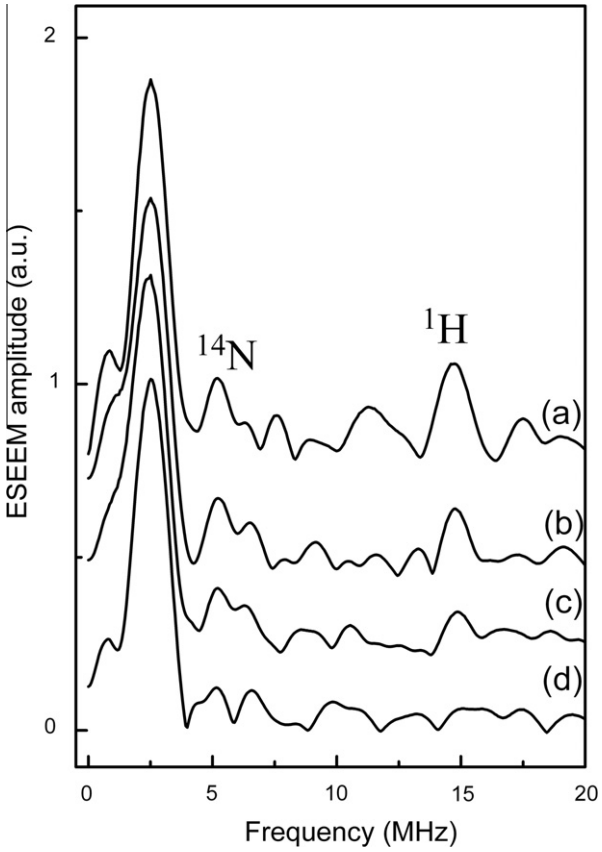

Fig. 8. Traces *a*, *b*, *c* and *d*, amplitude FT spectra of the PELDOR traces *a*, c, *d* in Fig. 7 and trace in Fig. 4B, respectively. The intensities are normalized by the amplitude of the 2.5 MHz peaks.

N, which results in the decrease of the mw amplitude in proportion with $(P/N)^{1/2}$. In the opposite case of a linear response of TWTA to the bandwidth expansion, the output power in one harmonic of a multifrequency pulse does not depend on the number of harmonics, so that the flip angles achieved for a single harmonic and multiple harmonics are similar. Clearly, the linear regime cannot be sustained for very long pulses or for very large number of harmonics, *N*, but it may be possible as a transient situation for a pulse with a limited bandwidth.

In order to decide, which of the regimes applies under the experimental conditions of this work, we have measured the dependence of the primary ESE signal of $Y_D^{\bullet}$ without and with the simultaneous application of the a multifrequency pulse consisting of five mw harmonic. The results of these measurements presented in Fig. 9 show that the mw amplitude in the mw harmonic in resonance with $Y_D^{\bullet}$ has decreased when the multifrequency pulses were applied, but this decrease was only within 15% (while for the model of completely saturated TWTA a 60% decrease was expected). We conclude therefore, that the regime of TWTA under the multifrequency excitation used in this work is actually somewhere between the completely saturated and linear.

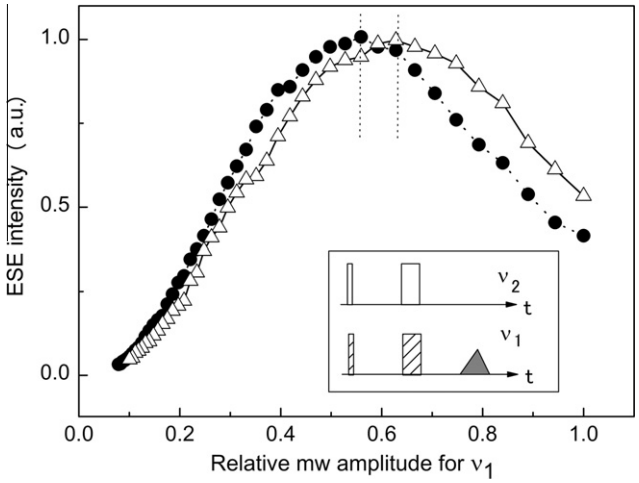

Fig. 9. The B_1-dependences of the primary ESE signal of $Y_D^{\bullet}$. The mw frequency (ν_1) in resonance with $Y_D^{\bullet}$ was supplied from original EPR bridge. Filled circles and open triangles show the ESE amplitudes for the measurements, respectively, without and with the simultaneous application of additional five-frequency (ν_2) mw pulses as shown in the inset. The ESE amplitudes were normalized by the maximum intensities. In the case of simultaneous application, the microwaves of ν_1 and ν_2 were combined in the mw bridge of the spectrometer. The horizontal axis shows the relative mw amplitude calculated from the attenuation level set by a mw attenuator between the TWTA and the resonator. The shift of the maximum of the dependence to the right (to smaller attenuations) thus corresponds to a smaller mw amplitude at a completely open attenuator. Dotted lines indicate the maxima corresponding to the $\pi/2-\tau-\pi$ sequences. *Inset* shows the pulse sequences. Experimental conditions: ν_1 = 9.60 GHz; ν_2 = 9.0 GHz × 2 and 10.0 GHz × 3, supplied from the multifrequency mw source; B_o = 343.0 mT; temperature, 4 K; pulse lengths, 16 and 24 ns; time interval between the pulses, τ = 200 ns.

With a linear regime, if all of the pumping pulse harmonics had a similar efficiency, the ELDOR effect would linearly depend on N, and the ratio 1:2:5 for the cases of $N = 1$, 2, and 5 would be seen. In reality, however, the mw harmonics constituting the pumping pulse are located at different offsets from the resonator optimum and have different efficiencies (turning angles), even if their amplitudes at the TWTA output are the same. This effect of the resonator and the non-linearity of TWTA regime result in the ratio of PELDOR amplitudes seen in the experiment.

With the linear TWTA regime, the ELDOR effect is obviously maximized for the pumping flip angle $\theta_o = \pi$, and this flip angle is the same for single-frequency or multifrequency excitation (only the bandwidths are different). Interestingly, for the saturated TWTA the same conclusion can be made. Indeed, for a pumping pulse with N frequency harmonics, the average amplitude in one harmonic and the nominal flip angle of the pumping pulse will be proportional to $(1/N)^{1/2}$. The bandwidth of this pulse, however, is proportional to N. The factor C in Eq. (1) (which determines the ELDOR amplitude) is thus proportional to:

$$C \propto N \cdot \sin^2\left(\theta_o/2\sqrt{N}\right) \tag{4}$$

where θ_o is the nominal flip angle for $N = 1$. For $\theta_o \sim \pi$ the factor C increases in proportion to N and reaches $(\pi/2)^2 \approx 2.47$ for $N \to \infty$. For $\theta_o \ll \pi$, on the other hand, no change in ELDOR amplitude should be observed because $N \cdot \sin^2(\theta_0/2\sqrt{N}) \approx N \cdot (\theta_0/2\sqrt{N})^2 \approx \theta_0^2/4$. It thus follows that in order to achieve an improvement of the ELDOR efficiency by using a multifrequency pumping pulse, regardless of the TWTA regime, the nominal flip angle of the pumping pulse for $N = 1$ should be close to π.

In summary, the use of a multifrequency pumping pulse in PELDOR has been investigated. It was found that such an approach can be used to improve the ELDOR effect by increasing the pumping bandwidth for the paramagnetic centers with broad EPR spectra. It is shown that the use of a multifrequency pumping can result in increased ELDOR effect if the nominal flip angle for a single-frequency pulse is close to π. The nuclear ESEEM was found to corrupt the PELDOR traces obtained with the pumping frequency being far from the resonator optimum, but it could be suppressed by using the τ-averaging.

Acknowledgments

This work was supported by grants from the Ministry of Education, Culture, Sports, Science and Technology of Japan (MEXT) (21370069 and 22654051) to H.M. and to M.I., Research Fellowship of the Japan Society for the Promotion of Science (JSPS) for Young Scientists (22005904) to R.M. Authors thank to Dr. Mizuno and coworkers (Nagoya University) for the help of measuring microwave power spectra.

References

[1] C.R. Timmel, J.E. Banham, C.M. Baker, S. Ceola, I.J. Day, G.H. Grant, E.J.J. Groenen, C.T. Rodgers, G. Jeschke, Distance measurements in the borderline region of applicability of CW EPR and DEER: a model study on a homologous series of spin-labelled peptides, J. Magn. Reson. 191 (2008) 202–218.
[2] J.B. Feix, C.S. Kiug, Site-directed spin labelling of membrane proteins and peptide–membrane interactions, in: L.J. Berliner (Ed.), Spin Labeling, PLENUM PRESS, New York and London, 1998, pp. 251–281.
[3] S. Saxena, J.H. Freed, Double quantum two-dimensional Fourier transform electron spin resonance: distance measurements, Chem. Phys. Lett. 251 (1996) 102–110.
[4] Y. Song, T.J. Meade, A.V. Astashkin, E.L. Klein, J.H. Enemark, A. Raitsimring, Pulsed dipolar spectroscopy distance measurements in biomacromolecules labeled with Gd(III) markers, J. Magn. Reson. 210 (2011) 59–68.
[5] I. Kaminker, M. Florent, B. Epel, D. Goldfarb, Simultaneous acquisition of pulse EPR orientation selective spectra, J. Magn. Reson. 208 (2011) 95–102.
[6] H. Hara, A. Kawamori, A.V. Astashkin, T. Ono, The distances from tyrosine D to redox-active components on the donor side of Photosystem II determined by pulsed electron–electron double resonance, Biochim. Biophys. Acta 1276 (1996) 140–146.
[7] D.A. Berthold, G.T. Babcock, C.F. Yocum, A Highly Resolved, Oxygen-evolving photosystem-II preparation from spinach thylakoid membranes – electron-paramagnetic-res and electron-transport properties, Febs. Lett. 134 (1981) 231–234.
[8] T. Ono, Y. Inoue, Effects of removal and reconstitution of the extrinsic 33, 24 and 16 KDa proteins on flash oxygen yield in photosystem-II particles, Biochim. Biophys. Acta 850 (1986) 380–389.
[9] H. Mino, A. Kawamori, T. Ono, Pulsed EPR studies of doublet signal and singlet-like signal in oriented Ca^{2+}-depleted PSII membranes: location of the doublet signal center in PSII, Biochemistry 39 (2000) 11034–11040.
[10] A.D. Milov, K.M. Salikohov, M.D. Shirov, Application of ENDOR in electron-spin echo for paramagnetic center space distribution in solids, Fiz. Tverd. Tela. 23 (1981) 975–982.
[11] A.D. Milov, A.B. Ponomarev, Y.D. Tsvetkov, Electron–electron double-resonance in electron-spin echo – model biradical systems and the sensitized photolysis of decalin, Chem. Phys. Lett. 110 (1984) 67–72.
[12] V.J. Derose, V.K. Yachandra, A.E. Mcdermott, R.D. Britt, K. Sauer, M.P. Klein, The state of manganese in the photosynthetic apparatus – nitrogen ligation to manganese in the photosynthetic oxygen-evolving complex – continuous-wave and pulsed Epr studies of photosystem II particles containing ^{14}N or ^{15}N, Biochemistry 30 (1991) 1335–1341.
[13] A.V. Astashkin, S.A. Dikanov, V.V. Kurshev, Y.D. Tsvetkov, Dependence of electron spin-echo modulation amplitude on the microwave field intensity, Chem. Phys. Lett. 136 (1987) 335–341.